biosensors

MDPI

Communication

Iodide-Mediated Etching of Gold Nanostar for the Multicolor Visual Detection of Hydrogen Peroxide

Yunping Lai †, Beirong Yu †, Tianran Lin * and Li Hou *

School of Chemistry and Pharmaceutical Sciences, State Key Laboratory for Chemistry and Molecular Engineering of Medicinal Resources, Guangxi Normal University, Guilin 541004, China; lyp159357@stu.gxnu.edu.cn (Y.L.); yubeirong@stu.gxnu.edu.cn (B.Y.)
* Correspondence: tianran@gxnu.edu.cn (T.L.); houli@gxnu.edu.cn (L.H.)
† These authors contributed equally to this work.

Abstract: A multicolor visual method for the detection of hydrogen peroxide (H_2O_2) was reported based on the iodide-mediated surface etching of gold nanostar (AuNS). First, AuNS was prepared by a seed-mediated method in a HEPES buffer. AuNS shows two different LSPR absorbance bands at 736 nm and 550 nm, respectively. Multicolor was generated by iodide-mediated surface etching of AuNS in the presence of H_2O_2. Under the optimized conditions, the absorption peak $\Delta\lambda$ had a good linear relationship with the concentration of H_2O_2 with a linear range from 0.67~66.67 μmol L^{-1}, and the detection limit is 0.44 μmol L^{-1}. It can be used to detect residual H_2O_2 in tap water samples. This method offered a promising visual method for point-of-care testing of H_2O_2-related biomarkers.

Keywords: iodide; gold nanostar; H_2O_2

1. Introduction

Hydrogen peroxide (H_2O_2) is widely used in fields such as the textile, chemical, environmental protection, medical, and food industries due to its ecological friendliness, strong oxidation ability, and ability to kill bacteria and bleach [1–4]. However, the direct addition of H_2O_2 in food production is prohibited by most countries, as residual H_2O_2 and its derived active substances can cause oxidative damage to human health [5,6]. Food-grade H_2O_2 residue is considered a "recognized safe substance" (JECFA, 2004), and according to the regulations of the Food and Agriculture Organization of the United States, the maximum concentration of H_2O_2 in dairy products is limited to 0.05%. In the Chinese national standard (GB53009.226-2016), the H_2O_2 content in food is strictly limited to less than 3 mg kg^{-1}. Excessive H_2O_2 may cause Alzheimer's, Parkinson's, amyotrophic lateral sclerosis, diabetes, traumatic brain injury, ischemia/reperfusion injury, learning and memory impairment, and other diseases [7–10]. Therefore, developing a simple and effective method to monitor H_2O_2 concentration is of great significance.

At present, the commonly used technologies for H_2O_2 detection include the colorimetric method [11–13], electrochemical method [14,15], fluorescence method [16,17], liquid chromatography [18,19], SERS [20,21], and others. Colorimetric detection has advantages in terms of simplicity, cost-effectiveness, and sensitivity in visual monitoring [22,23]. Most colorimetric methods used for H_2O_2 detection are based on the color reaction of substrate 3, 3, 5, 5,—tetramethylbenzidine (TMB) [22,24,25] and o-phenylenediamine (OPD) [26–28] oxidized by H_2O_2 under the action of a catalyst to quantify H_2O_2. However, these organic compounds are toxic and are easily oxidized by O_2. Therefore, developing a stable H_2O_2 detection method without chromogenic substrates is meaningful. Precious metal nanostructures have many excellent properties, such as good light scattering, absorption, and photothermal conversion capabilities [11,29]. Au NS is an uncommon type of gold nanostructure. In 2006, Nehl et al. [30] systematically studied gold nanostructures and multi-branched nanoparticles with sharp tips and unique local surface plasmon resonance

check for updates

Citation: Lai, Y.; Yu, B.; Lin, T.; Hou, L. Iodide-Mediated Etching of Gold Nanostar for the Multicolor Visual Detection of Hydrogen Peroxide. *Biosensors* **2023**, *13*, 585. https://doi.org/10.3390/bios13060585

Received: 5 May 2023
Revised: 24 May 2023
Accepted: 26 May 2023
Published: 28 May 2023

Copyright: © 2023 by the authors. Licensee MDPI, Basel, Switzerland. This article is an open access article distributed under the terms and conditions of the Creative Commons Attribution (CC BY) license (https://creativecommons.org/licenses/by/4.0/).

(LSPR) characteristics. Au NS is a promising choice for biosensor application due to its sharp corners, plasma resonance, and lightning rod effect [31,32]. Research has shown that the LSPR characteristics of Au NS are related to their size, shape, and composition. Chemical etching can change the length of the sharp angle of Au NS and the surface plasmon resonance of Au NS, which means that the chemical etching of the sharp angle of Au NS will shift the LSPR absorption peak of Au NS and produce a blue color change [12,13,33]. The etching process can be adjusted by iodide to quickly and sensitively generate the blue shift of the surface plasmon resonance spectrum [34].

Considering the important role of H_2O_2, this work intended to construct a multicolor sensor based on the reaction between H_2O_2, Au NS, and I^- (Scheme 1A). Firstly, H_2O_2 reacts with I^- to generate I_2 with the help of horseradish peroxidase (HRP). The remaining I^- etches the sharp corners of Au NS, which changes the absorption peak of LSPR shifts and the color of the solution. With the increasing concentration of I^-, the degree of blue shift ($\Delta\lambda$) increases. The color of the mixture changes from blue to purple and finally turns pink, and $\Delta\lambda$ can be used for the quantification of H_2O_2 (Scheme 1B).

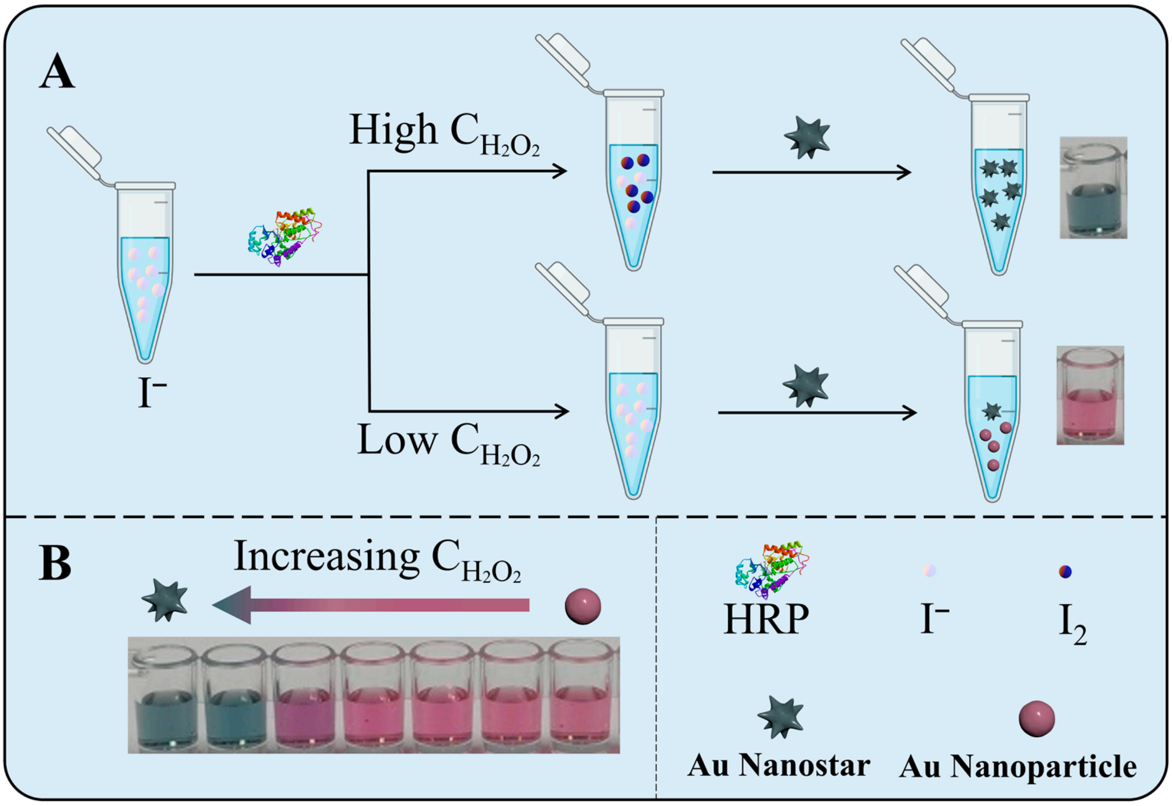

Scheme 1. Schematic illustration of iodide-mediated etching of Au NS for H_2O_2 detection (**A**) and color changes with increasing H_2O_2 (**B**).

2. Experimental Section

2.1. Reagents and Materials

Tetrachloroauric acid ($HAuCl_4$) and trisodium citrate dihydrate ($Na_3C_6H_5O_7{\cdot}2H_2O$) were purchased from Xilong Chemical Co., Ltd., Shantou, China; potassium iodide (KI) was purchased from Sinopharm Chemical Reagent Co., Ltd., Shanghai, China; H_2O_2, potassium chloride (KCl), potassium sulfate (K_2SO_4), and sodium nitrate (KNO_3) were purchased from Xilong Science Co., Ltd., Shantou, China; 4-(2-Hydroxyethyl)Piperazine-1-ethanesulfonic acid sodium salt (HEPES-Na), horseradish peroxidase (HRP), tris(hydroxymethyl) aminome thane (Tris), and sodium carbonate (Na_2CO_3) were purchased from Aladdin Co., Ltd., Fukuoka, Japan. All chemicals are analytical grade, and the solution is prepared using deionized water obtained from the Milli-Q water purification system ($\geq$18.2 M Ω cm^{-1}, Milli-Q, Millipore, Burlington, MA, USA).

2.2. Apparatus

The transmission electron microscope (FE-TEM) images of Au NS were collected by JEOL200 kV field emission transmission electron microscope (JEM-2100 F, JEOL, Tokyo, Japan). We used KQ5200DE ultrasonic cleaner (Kunshan Ultrasonic Instrument Co., Ltd., Kunshan, China) to perform ultrasonic treatment on the sample and the UV–Vis spectrum was recorded by using a Tecan Spark microplate reader (Tecan, Switzerland).

2.3. Synthesis of Au NS [34]

Golden Seed: Add a trisodium citrate solution (4 mL, 1%) to a rapidly stirred boiling $HAuCl_4$ aqueous solution (50 mL, 0.5 mmol L^{-1}) and boil for 30 min. The solution color changes from purple-red to wine-red. Then, cool the wine-red solution to room temperature to obtain the gold seed solution, and store it at 4 °C for later use.

Au NS: Take 750 µL seeds solution, vigorously stir and add 38.5 mL of water, 18.75 mL of HEPES-Na (100 mmol L^{-1}, pH = 8.5), and 750 µL hydroxylamine hydrochloride ($HONH_2HCl$, 40 mmol L^{-1}), then 22.5 mL of $HAuCl_4$ (1 mmol L^{-1}) was added to the above solution, and stir for 15 min to obtain a blue solution.

2.4. Detection of H_2O_2

After incubation at 37 °C for 40 min, 50 µL HRP (40 ng mL^{-1}), 100 µL KI and 100 µL H_2O_2 of different concentrations were added into 250 µL Tris-HCl (10 mmol L^{-1}, pH = 3.0) buffer solution. Take 50 µL and add it to 250 µL Au NS. After the reaction at 37 °C for 25 min, the ultraviolet absorption spectra of each pore were recorded by a Tecan microplate reader. The calibration curve of $\Delta\lambda$ and H_2O_2 concentration was constructed by drawing the wavelength shift change values ($\Delta\lambda$) of different concentrations of H_2O_2, where wavelength change value $\Delta\lambda = \lambda_0 - \lambda$ (λ_0 is the peak value of Au NS, λ is the peak value measured after the etching of Au NS).

2.5. Detection of H_2O_2 in Tap Water

A standard addition method was used to evaluate the feasibility of iodide-mediated Au NS etching for detecting H_2O_2 in tap water. Follow the above steps (drawing a standard curve) to determine the concentration of H_2O_2 in tap water by recording the change in wavelength offset ($\Delta\lambda$).

3. Results and Discussion

3.1. Characterization of AuNS

AuNS are synthesized by a seed-mediated method. First, small gold nanoparticles are synthesized, and then gold seeds are added to the growth solution containing $HAuCl_4$, a reducing agent, and surfactant. The newly reduced Au° grows on the surface of the seeds to form Au NS [18,35,36]. The UV–Vis spectrum measured using a Tecan microplate reader is shown in Figure 1A. The absorbance intensities of the Au NS solution at different wavelengths were recorded as the optical density (OD). It can be seen that the Au NS has two SRP bands located at 736 nm and 550 nm, respectively. λ_0 represents the maximum absorption peak of Au NS at 736 nm. Figure 1B shows that Au NS has multiple sharp edges. Compared to smooth surfaces, the multiple sharp edges of Au NS have special sensitivity to the etching of I^-, and iodide binds to the surface during the etching process [36]. After I^- etched Au NS, the sharp corners become shorter, and Au NS are etched into spherical nanostructures (Figure 1C). Due to the fact that gold atoms are "soft" Lewis acids, and I^- is a classic "soft" Lewis donor [34], iodide has a high affinity for gold. Oxidized Au ions and iodide can chelate at the interface of Au NS [37], resulting in uneven or even larger Au NS sizes after etching.

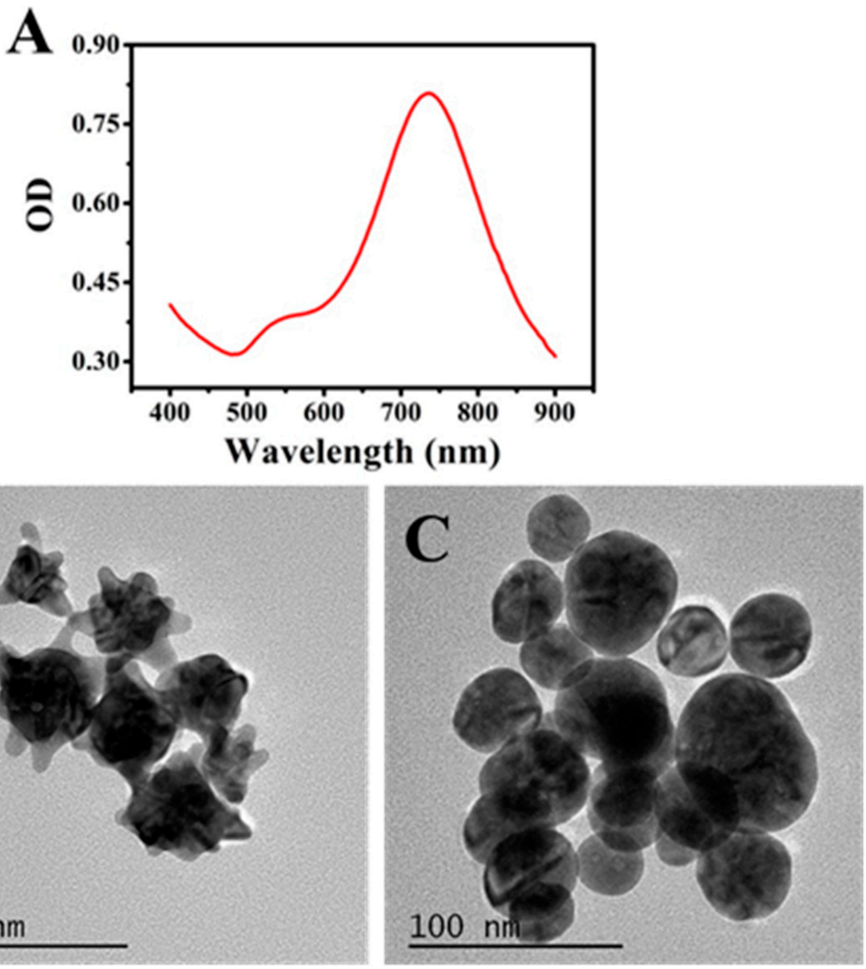

Figure 1. (**A**) UV–Vis spectrum of AuNS; (**B**) TEM images of AuNS before etching and (**C**) after etching.

3.2. Feasibility of Iodide-Mediated Etching of AuNS for Detecting H_2O_2

To investigate the feasibility of using iodide-mediated surface etching of AuNS for detecting H_2O_2, we first validated the UV–Vis spectra of different mixtures. As shown in Figure 2A,B, when only Au NS exists, the absorption peak was measured at 736 nm (Figure 2B, curve e). After adding a final concentration of I^- as 80 μmol L^{-1}, the peak of the UV visible absorption peak changed from 736 nm to 588 nm, resulting in a significant blue shift of the UV peak absorption peak (Figure 2B, curve d). The addition of H_2O_2 and HRP separately does not affect the etching of AuNS by I^- (curves b and c in Figure 2B). Only when both exist simultaneously does the absorption peak of the mixture shift to red (curve as in Figure 2B). This is because the addition of H_2O_2 or HRP alone into the reaction system does not affect the concentration of I^-, and all I^- is used for etching AuNS. After the addition of both, HRP can catalyze the oxidation of iodide to elemental iodine in the presence of H_2O_2 [34]. It led to a decrease in the remaining concentration of iodide. A decrease etching degree of Au NS was also observed which resulted in a red shift of the absorption peak of Au NS. In addition, we validated the relationship between the concentration of I^- and the degree of etching. When the concentration of I^- increases from 0 mmol L^{-1} to 1.2 mmol L^{-1}, the etching degree gradually increases and reaches the plateau (Figure 2D), and the corresponding absorption peak shifts from 736 nm to 556 nm. At the same time, the color of the solution changes from dark blue to purple to pink (Inset of Figure 2D). In Figure 2C, it can be seen that as the concentration of I^- increases from 0 mmol L^{-1} to 0.08 mmol L^{-1}, the etching degree gradually increases. When the concentration of I^- increases from 0.05 mmol L^{-1} to 0.06 mmol L^{-1}, the maximum absorption peak of the Au NS solution shows a large blue shift (Δλ). However, the increase in Δλ becomes little from 0.06 mmol L^{-1} to 0.08 mmol L^{-1}. Therefore, an I^- concentration of 0.06 mmol L^{-1} was selected for the sensitive detection of H_2O_2. The above experimental results indicate that this method based on the iodide-mediated etching of AuNS for detecting H_2O_2 has good feasibility.

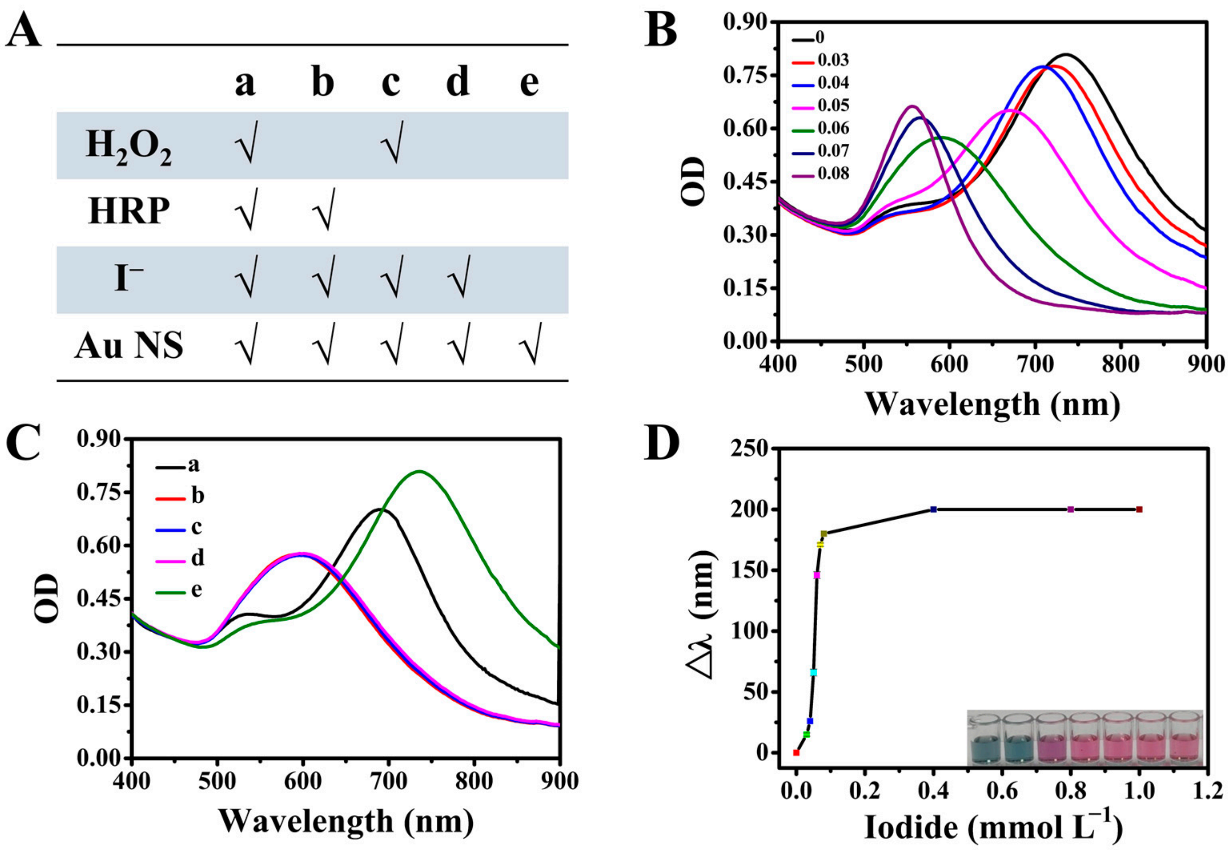

Figure 2. (**A**) Table of the solutions (a, b, c, d, e) with different components for the etching of AuNS. (**B**) The corresponding UV−Vis spectra of AuNS after etching with different components. (**C**) UV−Vis spectra of AuNS after etching by different concentrations of I^-. (**D**) The relationship between etching degree and I^- concentration. Inset is the color change with varying degrees of etching.

3.3. Optimization of Experimental Conditions

To obtain a more sensitive response, several parameters in the experimental system were optimized, such as the time for I^- etching AuNS, the incubation time for the reaction between HRP and H_2O_2, and the reaction temperature (Figure 3). As shown in Figure 3A, the reaction time for I^--induced etching of AuNS was optimized. After adding a concentration of 0.06 mmol L^{-1}, the plateau was reached with a reaction time of 25 min, indicating that the etching of AuNS by I^- can reach stability after 25 min. Figure 3B shows the optimization of incubation time for HRP and H_2O_2. At this point, the concentration of H_2O_2 is 33.3 μmol L^{-1}. As the time of HRP catalyzing H_2O_2 prolongs, the etching degree gradually decreases and reaches stability. This is because the amount of I^- consumed by H_2O_2 under HRP catalysis increases, resulting in a decrease in the remaining I^-, leading to a decrease in the degree of Au NS etching and a shift in the UV absorption peak. Finally, we optimized the reaction temperature. The experimental results indicate that an increase in temperature contributes to the etching of the reaction system (Figure 3C), but a higher temperature will reduce the catalytic efficiency of HRP. Therefore, we chose a reaction time of 25 min for I^--induced etching of AuNS, an incubation time of 40 min for the reaction between HRP and H_2O_2, and a reaction temperature of 37 °C.

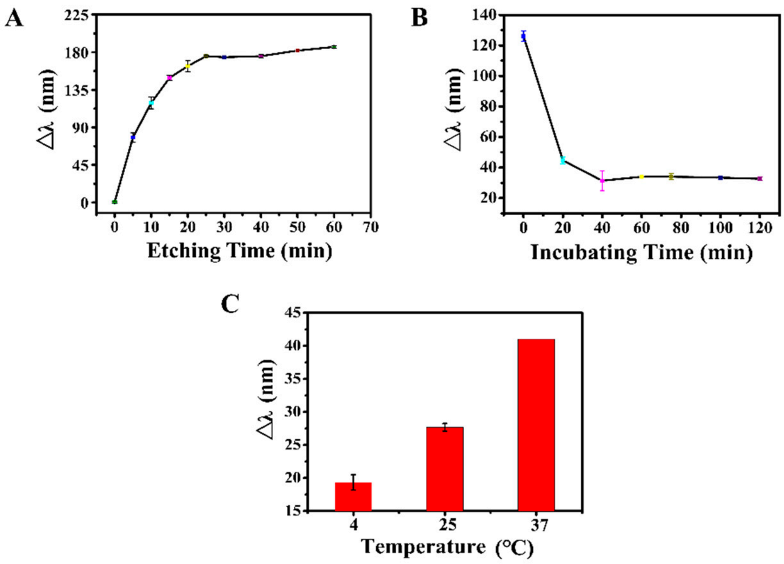

Figure 3. Optimization of (**A**) time for I^- etching of AuNS at 37 °C; (**B**) response time for the reaction between HRP and H_2O_2; (**C**) reaction temperature.

3.4. Performance Analysis of Iodide-Mediated AuNS Etching for Detecting H_2O_2

Under optimal experimental conditions, the linear response range and detection limit of H_2O_2 detected by the constructed sensor platform were investigated by monitoring the offset value of the absorption peak (Δλ). As shown in Figure 4A,B, with the increase in H_2O_2 concentration in the range of 0.67–66.67 μmol L^{-1}, Δλ gradually increases and reaches a plateau. In the range of 0.67–33.33 μmol L^{-1}, Δλ has a strong linear relationship with the concentration of H_2O_2 (Figure 4C). The linear equation is $\Delta\lambda = -2.84C_{H_2O_2} + 123.69$ ($R^2 = 0.9908$, $n = 3$) and the LOD value is 0.44 μmol L^{-1} ($n = 20$, $3\sigma_0/K$). Compared with other reported H_2O_2 sensors (Table S1), this method is rapid and sensitive, and shows a multicolor change which has great potential application in the field of point-of-care testing.

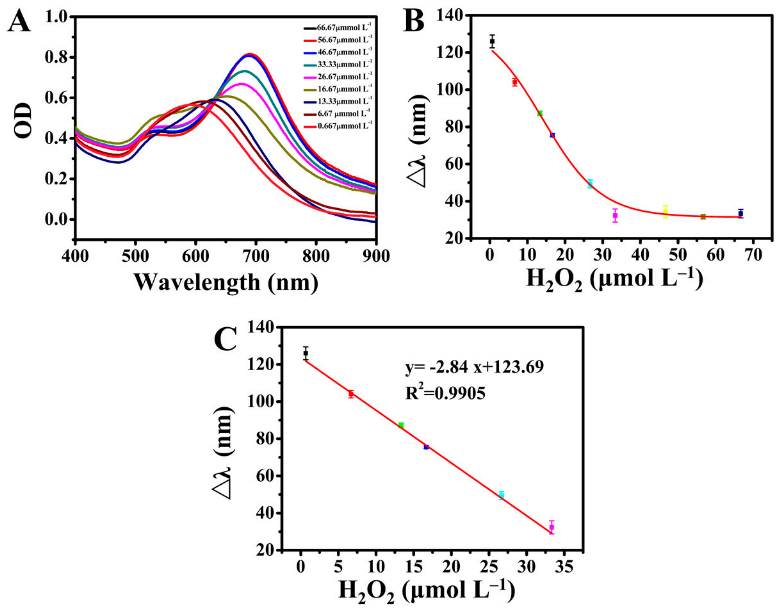

Figure 4. (**A**) UV–Vis spectra of iodide-mediated etching of AuNS in the presence of H_2O_2 with different concentrations. (**B**) The responses of Δλ to different concentrations of H_2O_2. (**C**) Linear relationship between Δλ and H_2O_2 concentration.

3.5. The Selectivity and Interference Study of Iodide-Mediated Etching of AuNS for Detecting H_2O_2

Tap water often contains a variety of salts, so it is necessary to explore the interference of different ions in the detection of hydrogen peroxide in tap water. To evaluate the selectivity and interference study of this method for H_2O_2 detection in tap water, six different interfering substances (K^+, Na^+, Cl^-, NO_3^-, SO_4^{2-}, CO_3^{2-},) were selected for the study. Figure 5A shows that under the same experimental conditions, except for H_2O_2, even if the concentration of other interfering substances is 50 times higher than the concentration of H_2O_2, the $\Delta\lambda$ shows no significant decrease. The above results indicate that this method has high selectivity for the detection of H_2O_2. Subsequently, we selected the above-mentioned interfering substances for the interference study. As shown in Figure 5B, the $\Delta\lambda$ value of H_2O_2 detection with the addition of interfering substances did not change. The results indicate that this method has good stability for detecting H_2O_2.

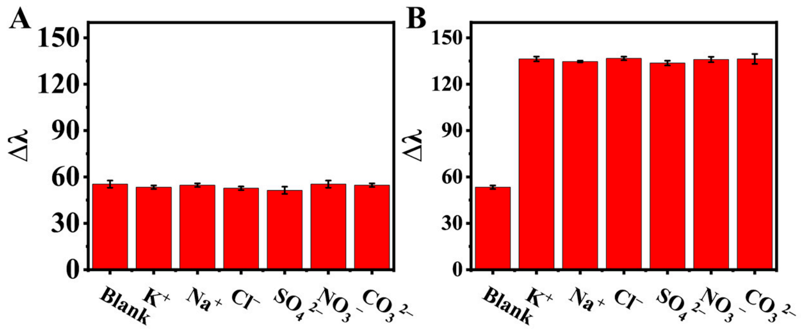

Figure 5. (**A**) The effect of (K^+, Na^+, Cl^-, NO_3^-, SO_4^{2-}, CO_3^{2-}) on the selectivity detection of H_2O_2. The concentration of H_2O_2 was 26.67 μmol L^{-1}. (**B**) The interference study for detecting H_2O_2.

3.6. Detection of H_2O_2 in Real Samples

To evaluate the potential applicability of this method for detecting H_2O_2 in real samples, tap water was selected as the actual sample, and the accuracy of the method was verified by the spiked recovery method. The specific experimental steps are as follows: Take 30% H_2O_2 and dilute it with tap water to different concentrations. Add 50 μL HRP (40 ng mL^{-1}) and 100 μL NaI to Tris-HCl (10 mmol L^{-1}, pH = 3.0) buffer solution. After incubating with 100 μL different concentrations of H_2O_2 at 37 °C for 40 min, 50 μL of the above solution was added to 250 μL Au NS, and the reaction was carried out at 37 °C for 25 min. UV measurement was performed after the reaction was completed. Unless otherwise specified, all detection experiments were independently repeated three times. Statistical analysis was conducted on the data obtained from at least three independent experiments. The data of all detection methods are represented as mean ± standard deviation (SD). The recovery rate of this method is between 92.8–101.6%, and the relative standard deviation (RSD) is between 3.4–4.4% (Table 1). These results indicated the superior accuracy and potential application of this method based on the iodide-mediated etching of AuNS for detecting H_2O_2.

Table 1. Detection of H_2O_2 in tap water samples.

Sample Number	Added (μmol L^{-1})	Found (μmol L^{-1})	Recovery (%)	RSD (n = 3, %)
1	10.0	9.28 ± 0.41	92.8	4.4
2	20.0	20.31 ± 0.70	101.6	3.5
3	30.0	28.18 ± 0.96	93.9	3.4

4. Conclusions

In this work, AuNS was utilized to construct a multicolor sensor for detecting H_2O_2 based on a rapid and sensitive surface etching of Au NS. AuNS are etched into spherical nanostructures in the presence of HRP, I^-, and H_2O_2. The etching process also produces color changes with different concentrations of H_2O_2 which can be used for visual detection. This method exhibits satisfactory sensitivity and selectivity. Under the conditions of an incubation time of 40 min, a reaction time of 25 min, a temperature of 37 °C, and I^- concentration of 0.06 mmol L^{-1}, the blue shift value of the absorption peak $\Delta\lambda$ shows a good linear relationship with the concentration of H_2O_2, with a linear range of 0.667~66.67 μmol L^{-1}, and a detection limit of 0.44 μmol L^{-1}. Because of the usage of the biological enzyme of HRP in this work, it is important to control the temperature during the analysis. This shortcoming might be solved by using a nanozyme to replace HRP. Considering the significant role of H_2O_2 in food chemistry and biochemistry, this work offered a new multicolor visual method for point-of-care testing and on-site analysis.

Supplementary Materials: The following supporting information can be downloaded at: https://www.mdpi.com/article/10.3390/bios13060585/s1, Table S1: comparative analysis of this method with other colorimetric methods for detecting H_2O_2. References [38–44] are cited in the Supplementary Materials.

Author Contributions: Conceptualization, Y.L.; methodology, Y.L.; validation, Y.L. and B.Y.; formal analysis, T.L.; investigation, Y.L. and B.Y.; writing—original draft preparation, Y.L. and T.L.; writing—review and editing, T.L. and L.H.; supervision, T.L.; project administration, T.L. and L.H.; funding acquisition, T.L. and L.H. All authors have read and agreed to the published version of the manuscript.

Funding: This research was funded by the Natural Science Foundation of Guangxi (2022GXNSFAA035475, 2023GXNSFAA026413) and the National Natural Science Foundation (22164005, 21964004).

Institutional Review Board Statement: Not applicable.

Informed Consent Statement: Not applicable.

Data Availability Statement: Not applicable.

Acknowledgments: The authors are grateful for financial support from the Natural Science Foundation of Guangxi and the National Natural Science Foundation.

Conflicts of Interest: The authors declare no conflict of interest.

References

1. Xing, L.; Zhang, W.; Fu, L.; Lorenzo, J.M.; Hao, Y. Fabrication and application of electrochemical sensor for analyzing hydrogen peroxide in food system and biological samples. *Food Chem.* **2022**, *385*, 132555. [CrossRef] [PubMed]
2. Mohiuddin, A.K.; Jeon, S. Highly efficient Ag doped δ-MnO_2 decorated graphene: Comparison and application in electrochemical detection of H_2O_2. *Appl. Surf. Sci.* **2022**, *592*, 153162. [CrossRef] [PubMed]
3. Gopakumar, A.; Ren, P.; Chen, J.; Manzolli Rodrigues, B.V.; Vincent Ching, H.Y.; Jaworski, A.; Doorslaer, S.V.; Rokicinska, A.; Kustrowski, P.; Barcaro, G.; et al. Lignin-Supported Heterogeneous Photocatalyst for the Direct Generation of H_2O_2 from Seawater. *J. Am. Chem. Soc.* **2022**, *144*, 2603–2613. [CrossRef] [PubMed]
4. Xue, Y.; Wang, Y.; Pan, Z.; Sayama, K. Electrochemical and Photoelectrochemical Water Oxidation for Hydrogen Peroxide Production. *Angew. Chem. Int. Ed.* **2021**, *60*, 10469–10480. [CrossRef] [PubMed]
5. Hu, Q.; Fang, Y.; Yu, X.; Huang, J.; Wang, L. A ferrocene-linked metal-covalent organic polymer as a peroxidase-enzyme mimic for dual channel detection of hydrogen peroxide. *Analyst* **2021**, *146*, 487–494. [CrossRef] [PubMed]
6. Zhang, Z.; Liu, Q.; Liu, Y.; Qi, R.; Zhou, L.; Li, Z.; Yun, J.; Liu, R.; Hu, Y. Colorimetric H_2O_2 Detection Using Ag-Nanoparticle-Decorated Silica Microspheres. *Nano* **2020**, *15*, 2050009. [CrossRef]
7. Liu, H.; Ding, Y.N.; Yang, B.C.; Liu, Z.X.; Zhang, X.; Liu, Q.Y. Iron Doped $CuSn(OH)_6$ Microspheres as a Peroxidase-Mimicking Artificial Enzyme for H_2O_2 Colorimetric Detection. *ACS Sustain. Chem. Eng.* **2018**, *6*, 14383–14393. [CrossRef]
8. Peng, Z.; Xiong, Y.; Liao, Z.; Zeng, M.; Zhong, J.; Tang, X.; Qiu, P. Rapid colorimetric detection of H_2O_2 in living cells and its upstream series of molecules based on oxidase-like activity of $CoMnO_3$ nanofibers. *Sens. Actuators B* **2023**, *382*, 133540. [CrossRef]
9. Ding, T.; Wang, Z.; Xia, D.; Zhu, J.; Huang, J.; Xing, Y.; Wang, S.; Chen, Y.; Zhang, J.; Cai, K. Long-Lasting Reactive Oxygen Species Generation by Porous Redox Mediator-Potentiated Nanoreactor for Effective Tumor Therapy. *Adv. Funct. Mater.* **2021**, *31*, 2008573. [CrossRef]
10. Meng, G.; Long, F.; Zeng, Z.; Kong, L.; Zhao, B.; Yan, J.; Yang, L.; Yang, Y.; Liu, X.Y.; Yan, Z.; et al. Silk fibroin based wearable electrochemical sensors with biomimetic enzyme-like activity constructed for durable and on-site health monitoring. *Biosens. Bioelectron.* **2023**, *228*, 115198. [CrossRef]

11. Zhang, Y.; Wang, G.; Yang, L.; Wang, F.; Liu, A. Recent advances in gold nanostructures based biosensing and bioimaging. *Coord. Chem. Rev.* **2018**, *370*, 1–21. [CrossRef]
12. Zeng, J.; Zhang, Y.; Zeng, T.; Aleisa, R.; Qiu, Z.; Chen, Y.; Huang, J.; Wang, D.; Yan, Z.; Yin, Y. Anisotropic plasmonic nanostructures for colorimetric sensing. *Nano Today* **2020**, *32*, 100855. [CrossRef]
13. Duan, W.; Liu, A.; Li, Q.; Li, Z.; Wen, C.Y.; Cai, Z.; Tang, S.; Li, X.; Zeng, J. Toward ultrasensitive and fast colorimetric detection of indoor formaldehyde across the visible region using cetyltrimethylammonium chloride-capped bone-shaped gold nanorods as "chromophores". *Analyst* **2019**, *144*, 4582–4588. [CrossRef] [PubMed]
14. Dong, H.; Zhou, Y.; Hao, Y.; Zhao, L.; Sun, S.; Zhang, Y.; Ye, B.; Xu, M. "Turn-on" ratiometric electrochemical detection of H_2O_2 in one drop of whole blood sample via a novel microelectrode sensor. *Biosens. Bioelectron.* **2020**, *165*, 112402. [CrossRef]
15. Xia, C.; He, W.; Yang, X.F.; Gao, P.F.; Zhen, S.J.; Li, Y.F.; Huang, C.Z. Plasmonic Hot-Electron-Painted Au@Pt Nanoparticles as Efficient Electrocatalysts for Detection of H_2O_2. *Anal. Chem.* **2022**, *94*, 13440–13446. [CrossRef]
16. Johnson, R.E.; van der Zalm, J.M.; Chen, A.; Bell, I.J.; Van Raay, T.J.; Al-Abdul-Wahid, M.S.; Manderville, R.A. Unraveling the Chemosensing Mechanism by the 7-(Diethylamino)coumarin-hemicyanine Hybrid: A Ratiometric Fluorescent Probe for Hydrogen Peroxide. *Anal. Chem.* **2022**, *94*, 11047–11054. [CrossRef]
17. Zhao, D.; Huang, Y.; Ouyang, H.; Shi, B.; Li, S.; Chen, S.; Zhao, S. Facile preparation of Cu-doped carbon dots for naked-eye discrimination of phenylenediamine isomers and highly sensitive ratiometric fluorescent detection of H_2O_2. *Talanta* **2022**, *239*, 123110. [CrossRef]
18. Liu, X.-L.; Wang, J.-H.; Liang, S.; Yang, D.-J.; Nan, F.; Ding, S.-J.; Zhou, L.; Hao, Z.-H.; Wang, Q.-Q. Tuning Plasmon Resonance of Gold Nanostars for Enhancements of Nonlinear Optical Response and Raman Scattering. *J. Phys. Chem. C* **2014**, *118*, 9659–9664. [CrossRef]
19. Chakraborty, A.; Acharya, H. Magnetically separable Fe_3O_4 NPs/MIL-53(Al) nanocomposite catalyst for intrinsic OPD oxidation and colorimetric hydrogen peroxide detection. *Colloids Surf. A Physicochem. Eng. Asp.* **2021**, *624*, 126830. [CrossRef]
20. Wu, L.; Zhou, X.; Wan, G.; Shi, S.; Wang, G. $NiFe_2O_4$/CNTs fabricated by atomic layer deposition as highly stable peroxidase mimics for sensitive colorimetric detection of hydrogen peroxide and glucose. *Mater. Res. Bull.* **2022**, *147*, 111637. [CrossRef]
21. Tran, H.V.; Nguyen, T.V.; Nguyen, L.T.N.; Hoang, H.S.; Huynh, C.D. Silver nanoparticles as a bifunctional probe for label-free and reagentless colorimetric hydrogen peroxide chemosensor and cholesterol biosensor. *J. Sci. Adv. Mater. Devices* **2020**, *5*, 385–391. [CrossRef]
22. Ahmed, A.; John, P.; Nawaz, M.H.; Hayat, A.; Nasir, M. Zinc-Doped Mesoporous Graphitic Carbon Nitride for Colorimetric Detection of Hydrogen Peroxide. *ACS Appl. Nano Mater.* **2019**, *2*, 5156–5168. [CrossRef]
23. Wang, H.-B.; Li, Y.; Dong, G.-L.; Gan, T.; Liu, Y.-M. A convenient and label-free colorimetric assay for dopamine detection based on the inhibition of the Cu(II)-catalyzed oxidation of a 3,3′,5,5′-tetramethylbenzidine—H_2O_2 system. *New J. Chem.* **2017**, *41*, 14364–14369. [CrossRef]
24. Li, L.; Liu, X.; Zhu, R.; Wang, B.; Yang, J.; Xu, F.; Ramaswamy, S.; Zhang, X. Fe^{3+}-Doped Aminated Lignin as Peroxidase-Mimicking Nanozymes for Rapid and Durable Colorimetric Detection of H_2O_2. *ACS Sustain. Chem. Eng.* **2021**, *9*, 12833–12843. [CrossRef]
25. Chen, H.; Shi, Q.; Deng, G.; Chen, X.; Yang, Y.; Lan, W.; Hu, Y.; Zhang, L.; Xu, L.; Li, C.; et al. Rapid and highly sensitive colorimetric biosensor for the detection of glucose and hydrogen peroxide based on nanoporphyrin combined with bromine as a peroxidase-like catalyst. *Sens. Actuators B* **2021**, *343*, 130104. [CrossRef]
26. Liu, Y.; Lopes, R.P.; Lüdtke, T.; Di Silvio, D.; Moya, S.; Hamon, J.-R.; Astruc, D. "Click" dendrimer-Pd nanoparticle assemblies as enzyme mimics: Catalytic o-phenylenediamine oxidation and application in colorimetric H_2O_2 detection. *Inorg. Chem. Front.* **2021**, *8*, 3301–3307. [CrossRef]
27. Ismail, S.M.; Abd-Elaal, A.A.; Abd El-salam, F.H.; Taher, F.A.; Aiad, I.; Shaban, S.M. Synthesis of silver decorated magnetic Fe_3O_4/alginate polymeric surfactant with controllable catalytic activity toward p-NP removal and enzymatic-mimic activity for solid-colorimetric H_2O_2 detection. *Chem. Eng. J.* **2023**, *453*, 139593. [CrossRef]
28. Wang, L.; Liu, Y.; Yang, Z.; Wang, Y.; Rao, H.; Yue, G.; Wu, C.; Lu, C.; Wang, X. A ratiometric fluorescence and colorimetric dual-mode assay for H_2O_2 and xanthine based on Fe, N co-doped carbon dots. *Dye. Pigment.* **2020**, *180*, 108486. [CrossRef]
29. Amjadi, M.; Abolghasemi-Fakhri, Z. Gold nanostar-enhanced chemiluminescence probe for highly sensitive detection of Cu(II) ions. *Sens. Actuators B* **2018**, *257*, 629–634. [CrossRef]
30. Nehl, C.L.; Liao, H.; Hafner, J.H. Optical properties of star-shaped gold nanoparticles. *Nano Lett.* **2006**, *6*, 683–688. [CrossRef]
31. Luo, L.; Luo, S.Z.; Jia, B.Z.; Zhang, W.F.; Wang, H.; Wei, X.Q.; Shen, Y.D.; Lei, H.T.; Xu, Z.L.; Yang, J.Y. A high-resolution colorimetric immunoassay for tyramine detection based on enzyme-enabled growth of gold nanostar coupled with smartphone readout. *Food Chem.* **2022**, *396*, 133729. [CrossRef] [PubMed]
32. Yu, Y.; Li, Y.; Zhang, Q.; Zha, Y.; Lu, S.; Yang, Y.; Li, P.; Zhou, Y. Colorimetric immunoassay via smartphone based on Mn^{2+}-Mediated aggregation of AuNPs for convenient detection of fumonisin B1. *Food Control.* **2022**, *132*, 108481. [CrossRef]
33. Mulder, D.; Phiri, M.M.; Vorster, B.C. Tailor-made gold nanostar colorimetric detection determined by morphology change and used as an indirect approach by using hydrogen peroxide to determine glucose concentration. *Sens. Bio-Sens. Res.* **2019**, *25*, 100296. [CrossRef]
34. Xianyu, Y.; Lin, Y.; Chen, Q.; Belessiotis-Richards, A.; Stevens, M.M.; Thomas, M.R. Iodide-Mediated Rapid and Sensitive Surface Etching of Gold Nanostars for Biosensing. *Angew. Chem. Int. Ed.* **2021**, *60*, 9891–9896. [CrossRef]

35. Tanwar, S.; Haldar, K.K.; Sen, T. DNA Origami Directed Au Nanostar Dimers for Single-Molecule Surface-Enhanced Raman Scattering. *J. Am. Chem. Soc.* **2017**, *139*, 17639–17648. [CrossRef]
36. Lin, M.-H.; Sun, L.; Kong, F.; Lin, M. Rapid detection of paraquat residues in green tea using surface-enhanced Raman spectroscopy (SERS) coupled with gold nanostars. *Food Control.* **2021**, *130*, 108280. [CrossRef]
37. Weng, G.; Dong, X.; Li, J.; Zhao, J. Halide ions can trigger the oxidative etching of gold nanorods with the iodide ions being the most efficient. *J. Mater. Sci.* **2016**, *51*, 7678–7690. [CrossRef]
38. Vetr, F.; Moradi-Shoeili, Z.; Özkar, S. Oxidation of o-phenylenediamine to 2,3-diaminophenazine in the presence of cubic ferrites MFe_2O_4 (M = Mn, Co, Ni, Zn) and the application in colorimetric detection of H_2O_2. *Appl. Organomet Chem.* **2018**, *32*, e4465. [CrossRef]
39. Vetr, F.; Moradi-Shoeili, Z.; Özkar, S. Mesoporous $MnCo_2O_4$ with efficient peroxidase mimetic activity for detection of H_2O_2. Inorg. *Chem. Commun.* **2018**, *98*, 184–191. [CrossRef]
40. Kong, J.; Zheng, J.; Li, Z.; Huang, J.; Cao, F.; Zeng, Q.; Li, F. One-pot synthesis of AuAgPd trimetallic nanoparticles with peroxidase-like activity for colorimetric assays. *Anal. Bioanal. Chem.* **2021**, *413*, 5383–5393. [CrossRef]
41. Zhu, D.; He, P.; Kong, H.; Yang, G.; Luan, X.; Wei, G. Biomimetic graphene-supported ultrafine platinum nanowires for colorimetric and electrochemical detection of hydrogen peroxide. *J. Mater. Chem. B* **2022**, *10*, 9216–9225. [CrossRef] [PubMed]
42. Liu, Y.; Yan, J.; Huang, Y.; Sun, Z.; Zhang, H.; Fu, L.; Li, X.; Jin, Y. Single-Atom Fe-Anchored Nano-Diamond with Enhanced Dual-Enzyme Mimicking Performance for H_2O_2 and Glutathione Detection. *Front. Bioeng. Biotechnol.* **2021**, *9*, 790849. [CrossRef] [PubMed]
43. Lu, W.; Chen, S.; Zhang, H.; Qiu, J.; Liu, X. Fe N C single atom nanozymes with dual enzyme-mimicking activities for colorimetric detection of hydrogen peroxide and glutathione. *J. Materiomics* **2022**, *8*, 1251–1259. [CrossRef]
44. Peng, L.-J.; Zhou, H.-Y.; Zhang, C.-Y.; Yang, F.-Q. Study on the peroxidase-like activity of cobalt phosphate and its application in colorimetric detection of hydrogen peroxide. *Colloids Surf. A Physicochem. Eng. Asp.* **2022**, *647*, 129031. [CrossRef]

Disclaimer/Publisher's Note: The statements, opinions and data contained in all publications are solely those of the individual author(s) and contributor(s) and not of MDPI and/or the editor(s). MDPI and/or the editor(s) disclaim responsibility for any injury to people or property resulting from any ideas, methods, instructions or products referred to in the content.